Science Advances
AAAS

advances.sciencemag.org/cgi/content/full/6/22/eaaz9014/DC1

Supplementary Materials for

Platelet-derived porous nanomotor for thrombus therapy

Mimi Wan*, Qi Wang, Rongliang Wang, Rui Wu, Ting Li, Dan Fang, Yangyang Huang, Yueqi Yu, Leyi Fang, Xingwen Wang, Yinghua Zhang, Zhuoyue Miao, Bo Zhao, Fenghe Wang, Chun Mao*, Qing Jiang, Xingquan Xu, Dongquan Shi*

*Corresponding author. Email: wanmimi@njnu.edu.cn (M.W.); maochun@njnu.edu.cn (C.M.); shidongquan1215@163.com (D.S.)

Published 27 May 2020, *Sci. Adv.* **6**, eaaz9014 (2020)
DOI: 10.1126/sciadv.aaz9014

The PDF file includes:

Other Supplementary Material for this manuscript includes the following:

(available at advances.sciencemag.org/cgi/content/full/6/22/eaaz9014/DC1)

Movie S1. Motion behavior of MMNM/PM nanomotors with NIR irradiation (9 s).

Movie S2. Motion behavior of MMNM-Cy5.5/PM nanomotors under fluorescent floating fibrin clots with NIR irradiation (5 s) (Green color: fluorescent floating fibrin clots stained by FITC, Red color: nanomotors stained with Cy5.5).

The photothermal conversion efficiency of MMNM was calculated according to the formula reported in previous literatures (*45*). According to the conservation of energy in the system, the following formula (1) can be obtained:

$$\sum_{i} m_i C_{p,i} \frac{dT}{dt} = Q_{NPs} + Q_s - Q_{loss} \qquad (1)$$

Here, m represents the mass, C_p is for heat capacity, T is the temperature, respectively. The subscript i of m and C_p refers to solvent water or nanoparticles (nanomotors in this work). Q_{NPs}, Q_s and Q_{loss} are the photothermal energy inputs by the nanomotors, the photothermal absorbed by the solvent per second, and the heat lost to the environment.

The specific formula to calculate Q_{NPs} is as follows:

$$Q_{NPs} = I(1-10^{-A_\lambda})\eta \qquad (2)$$

Where I is the laser power, A_λ is the absorbance of nanomotors under the wavelength of 808 nm, η is composed of light energy into heat energy conversion efficiency of field.

$$Q_{loss} = hA\Delta T \qquad (3)$$

h is the heat transfer coefficient, A is the surface area of container, ΔT is the temperature change between the temperature in solution (T) and environmental temperature (T_{surr}).

$$Q_s = Q_{loss} = hA\Delta T_{max,H_2O} \qquad (4)$$

When the system reaches its maximum steady-state temperature, the output heat is equal to the input heat, so

$$Q_{NPs} + Q_s = Q_{loss} = hA\Delta T_{max,mix} \qquad (5)$$

According to formula (2), (4) and (5) above, the formula of photothermal conversion efficiency can be converted as follows

$$\eta = \frac{hA\Delta T_{max,mix} - hA\Delta T_{max,H_2O}}{I(1-10^{-A_\lambda})} = \frac{hA(\Delta T_{max,mix} - \Delta T_{max,H_2O})}{I(1-10^{-A_\lambda})} \qquad (6)$$

hA can be obtained from the following formula (*46*):

$$t = -\frac{\sum_i m_i C_{p,i}}{hA}\ln\theta = -\frac{\sum_i m_i C_{p,i}}{hA}\ln\left(\frac{T - T_{surr}}{T_{max} - T_{surr}}\right) \qquad (7)$$

Where, t is the solution cooling time (s). We fit it linearly to t and -lnθ in fig. S25, and the slope is 293.22, that is $\frac{\sum_i m_i C_{p,i}}{hA}$. Since the values of m_{NPs} and C_{NPs} are very small, they are considered negligible. So, $C_{solvent}$ is the heat capacity of the water (4.2 J g^{-1} $°C^{-1}$), m is the quality of the solution (1 g), *hA* can be calculated to be equal to 0.0143.

According to formula (6), $\Delta T_{max,mix}$ is 16.9 °C, $\Delta T_{max,H_2O}$ is 1.4 °C, A_λ is 0.586, and finally the calculated photothermal conversion efficiency of the nanomotor is 11.96%.

Table S1. Physical properties of different samples.

Sample	S (m^2g^{-1})	Vp (cm^3g^{-1})	D (nm)	
			mesopore	macropore
MS	237.1	0.585	3.59	---
MMS	604.1	0.771	5.10	58
MMNM	415.7	0.690	3.59	40
MMNM/Hep	170.9	0.345	3.00	44
MMNM/Hep/UK	10.2	0.034	3.00	31
MMNM/Hep/UK/PM	9.4	0.004	---	31

Table S2. Linear fitting parameters for MSD plot of nanomotors with NIR irradiation under different power densities (y = a + bx).

	Power density (W cm^{-2})	R^2	a	b
NIR	0.5	0.9212	-6.93	6.71
	1	0.8740	-2.02	7.22
	1.5	0.9310	-144.71	101.82
	2	0.9107	-304.49	188.62

Table S3. Parabolic fitting parameters for MSD plot of nanomotors with NIR irradiation under different power densities ($y = ax^2 + bx + c$).

	Power density (W cm^{-2})	R^2	a	b	c
NIR	0.5	0.9357	0.36	3.49	-2.15
	1	0.8747	0.08	8.00	-3.18
	1.5	0.9934	11.18	0.80	7.84
	2	0.9952	24.44	-31.56	22.51

Table S4. Power function fitting parameters for MSD plot of nanomotors with NIR irradiation under different power densities ($y = ax^b$).

	Power density (W cm^{-2})	R^2	a	b
NIR	0.5	0.9361	2.22	1.49
	1	0.8696	6.30	1.05
	1.5	0.9930	12.59	1.95
	2	0.9957	13.16	2.22

Table S5. Parameters and coefficients obtained for Zero-order release model $Q_t = K_0t$, First-order release model $ln(1-Q_t/Q_f) = -K_1t$ and Peppas release model $ln(M_t/M_\infty) = lna + blnt$ fitted to the UK release profiles from MMNM/UK and Hep release profiles from MMNM/Hep.

Release models	Release parameters	UK	Hep
Zero order	K_0	26.65	2.84
	R^2	0.7251	0.7943
First order	K_1	1.47	0.22
	R^2	0.9324	0.9754
Peppas	a	0.74	0.25
	b	0.31	0.54
	R^2	0.9913	0.9526

Table S6. Parameters and coefficients obtained for Zero-order release model $Q_t = K_0t$, First-order release model $ln(1-Q_t/Q_f) = -K_1t$ and Peppas release model $ln(M_t/M_\infty) = lna + blnt$ fitted to the UK and Hep release profiles from MMNM/Hep/UK/PM under NIR irradiation.

Release models	Release parameters	UK	Hep
Zero order	K_0	28.89	3.33
	R^2	0.8849	0.7805
First order	K_1	1.12	0.22
	R^2	0.9028	0.9593
Peppas	a	0.59	0.36
	b	0.50	0.37
	R^2	0.9943	0.9939

Table S7. The Pt amount in major organs of the rat treated with different samples.

Sample	Time (d)	Heart (mg/g)	Lung (mg/g)	Kidney (mg/g)	Liver (mg/g)	Spleen (mg/g)
MMNM/UK	3	< 0.0001	< 0.0001	< 0.0001	0.0002	< 0.0001
	7	< 0.0001	< 0.0001	0.002	0.0006	< 0.0001
MMNM/Hep	3	< 0.0001	< 0.0001	< 0.0001	0.0002	< 0.0001
	7	< 0.0001	< 0.0001	0.001	0.0006	< 0.0001
MMNM/Hep/UK	3	< 0.0001	< 0.0001	0.0002	0.0003	< 0.0001
	7	< 0.0001	< 0.0001	0.0004	0.0008	< 0.0001
MMNM/Hep/UK/PM	3	< 0.0001	< 0.0001	< 0.0001	0.0005	< 0.0001
	7	< 0.0001	< 0.0001	0.0005	0.0004	< 0.0001

Table S8. The Pt amount in major organs of the rat treated with MMNM/Hep/UK/PM under NIR irradiation.

Time (d)	Heart (mg g^{-1})	Lung (mg g^{-1})	Kidney (mg g^{-1})	Liver (mg g^{-1})	Spleen (mg g^{-1})
1	< 0.0001	< 0.0001	< 0.0001	< 0.0001	< 0.0001
3	< 0.0001	< 0.0001	0.002	0.001	< 0.0001
7	< 0.0001	< 0.0001	0.001	0.001	< 0.0001

Table S9. Blood routine analysis of rats after being treated with different samples for 7 d.

Group	PBS	Nanomotors
Percentage of monocytes	2.8±0.78	2.2±0.29
Neutrophil count	0.5±0.21	0.2±0.07
Red blood cell count	7.85±0.49	7.26±0.25
Hemoglobin (HGB)	151±5.66	138±0.71
Hematocrit (HCT)	45.2±3.04	42.7±0.57
Mean corpuscular volume (MCV)	58.0±0.28	58.8±1.27
Mean hemoglobin content (MHC)	19.2±0.14	19.0±0.57
Mean corpuscular hemoglobin concentration (MCHC)	321±2.12	323±2.83
RBC volume distributing width (RDW)	14.7±0.14	15.1±1.48

Table S10. Values of serum enzymes in blood of rats after being treated with different samples for 7 d.

Group	PBS	Nanomotors
Cholinesterase (CHE)	0.2±0.07	0.2±0.07
Total Protein (TP)	59.2±2.55	57.1±2.33
Albumin	31.0±0.35	30.3±0.99
Globulin	28.2±0.35	25.4±1.34
Ratio of albumin to globulin	1.19±0.05	1.25±0.03
Glucose	8.92±0.21	9.75±0.59
Urea	6.7±0.21	6.6±0.21
Creatinine	25±2.12	27±2.29
Total carbon dioxide	21.8±0.42	22.1±1.56
Cholesterol	1.53±0.09	1.57±0.32
H-cholesterol	1.22±0.02	1.30±0.28
L-cholesterol	0.51±0.01	0.51±0.02
Apolipoprotein B	0.01±0.00	0.01±0.00
Total calcium	2.98±0.08	2.96±0.02
Phosphorus	2.86±0.10	2.70±0.18
Potassium	6.58±0.20	6.56±0.06
Sodium	139.4±1.13	138.6±1.98
Chlorine	95.0±2.05	96.4±1.63

Table S11. Blood routine analysis of rats after being treated with different samples for 25 d.

Group	PBS	Nanomotors
Percentage of monocytes	7.2±5.09	6.3±0.49
Neutrophil count	0.1±0.00	0.1±0.07
Red blood cell count	9.18±0.36	8.09±0.32
Hemoglobin (HGB)	187±2.42	161±2.12
Hematocrit (HCT)	51.8±0.80	45.7±0.71
Mean corpuscular volume (MCV)	58.7±1.63	59.2±0.42
Mean hemoglobin content (MHC)	20.9±0.35	20.9±0.14
Mean corpuscular hemoglobin concentration (MCHC)	355±4.24	354±0.71
RBC volume distributing width (RDW)	13.5±0.67	15.7±0.78

Table S12. Values of serum enzymes in blood of rats after being treated with different samples for 25 d.

Group	PBS	Nanomotors
Cholinesterase (CHE)	0.1±0.00	0.1±0.00
Total Protein (TP)	61.8±0.79	61.7±0.78
Albumin	36.1±0.28	36.2±0.28
Globulin	24.3±0.99	24.4±1.20
Ratio of albumin to globulin	1.4±0.01	1.35±0.01
Glucose	12.33±3.30	11.66±0.23
Urea	6.5±0.28	6.7±0.28
Creatinine	22±0.71	27±0.71
Total carbon dioxide	15.9±0.28	15.8±0.85
Cholesterol	1.42±0.20	1.36±0.13
H-cholesterol	1.00±0.10	0.99±0.12
L-cholesterol	0.21±0.06	0.22±0.03
Apolipoprotein B	0.01±0.00	0.01±0.00
Total calcium	3.12±0.05	3.09±0.07
Phosphorus	2.21±0.30	2.18±0.01
Potassium	11.52±0.02	9.51±0.28
Sodium	135.7±2.47	134.7±1.70
Chlorine	99.3±2.12	99.2±0.42

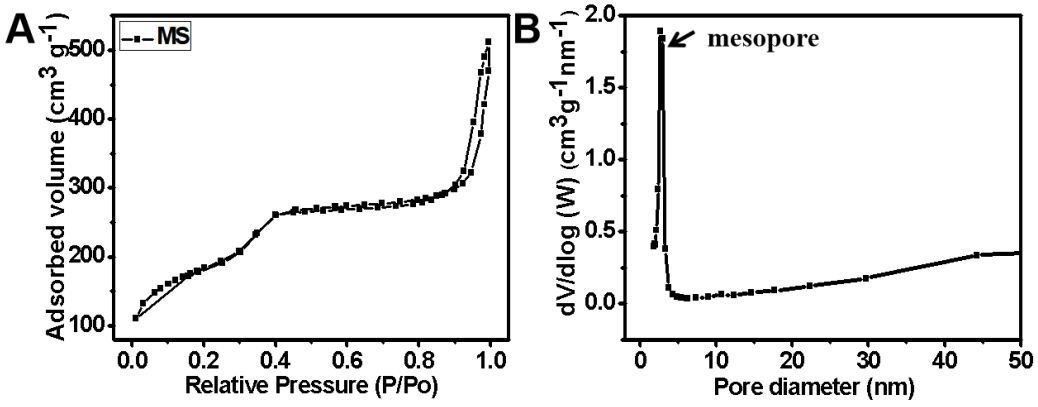

Fig. S1. Pore structure characterization of MS. (A) N_2 adsorption-desorption isotherms and (B) BJH pore size distribution curves of MS.

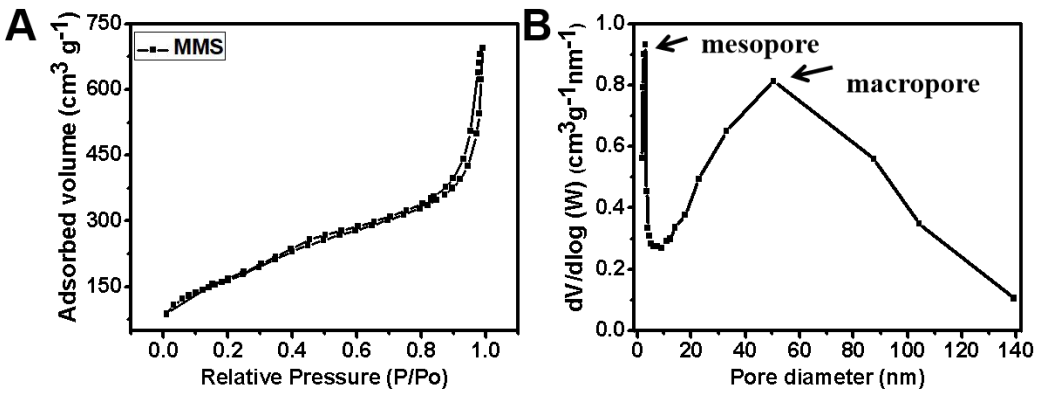

Fig. S2. Pore structure characterization of MMS. (A) N_2 adsorption-desorption isotherms and (B) BJH pore size distribution curves of MMS.

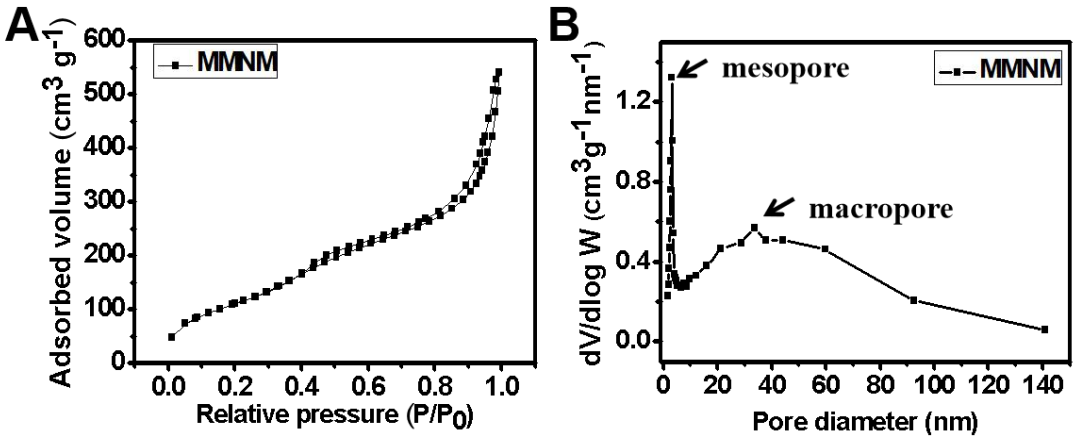

Fig. S3. Pore structure characterization of MMNM. (A) N_2 adsorption-desorption isotherms and (B) BJH pore size distribution curves of MMNM.

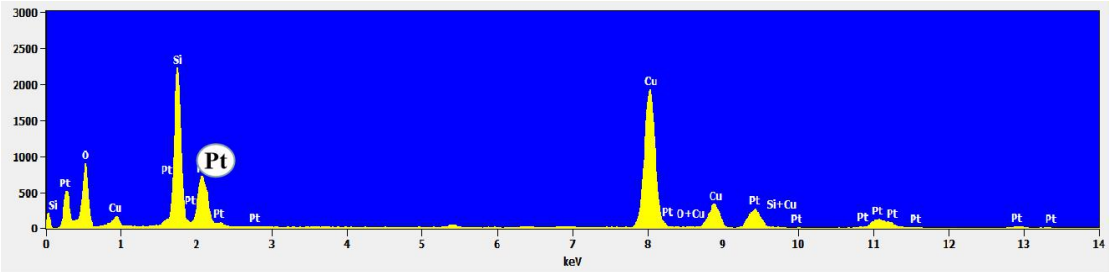

Fig. S4. EDS spectrum of MMNM.

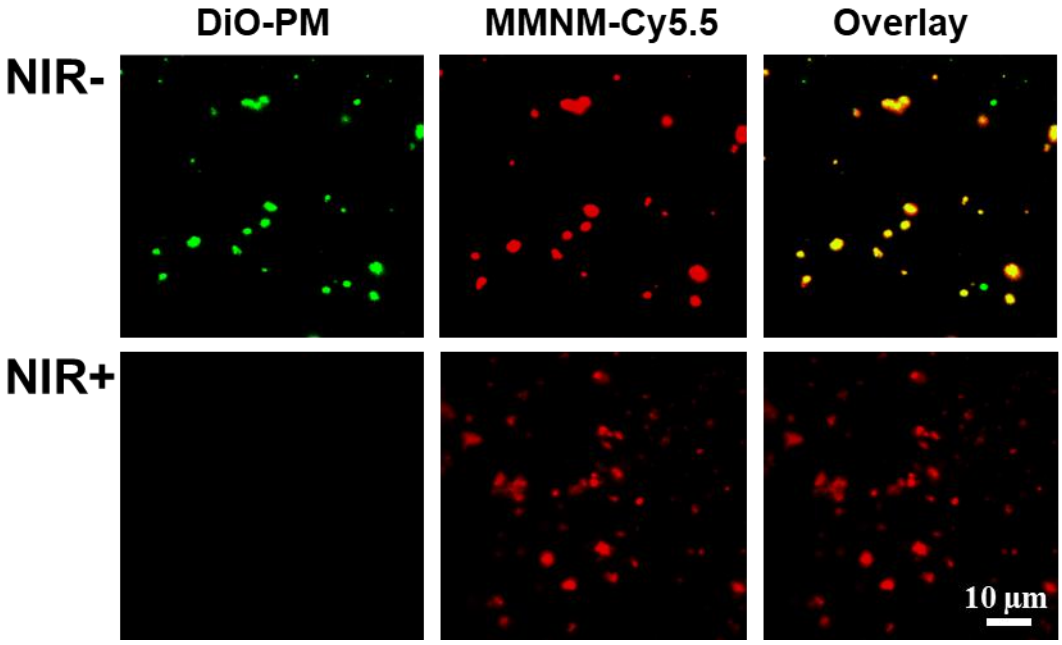

Fig. S5. Colocalization of PM stained with DiO (green) and MMNM stained with Cy5.5 (red) by CLSM observation (Scale bar: 10 μm).

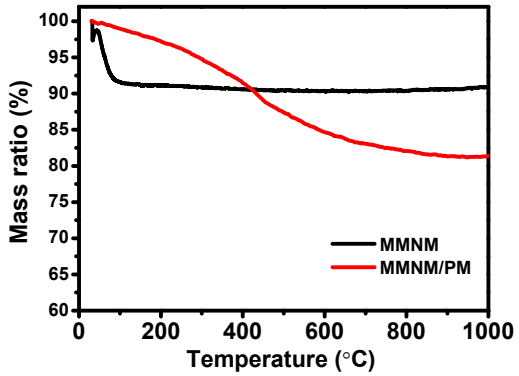

Fig. S6. TG measurement of MMNM and MMNM/PM.

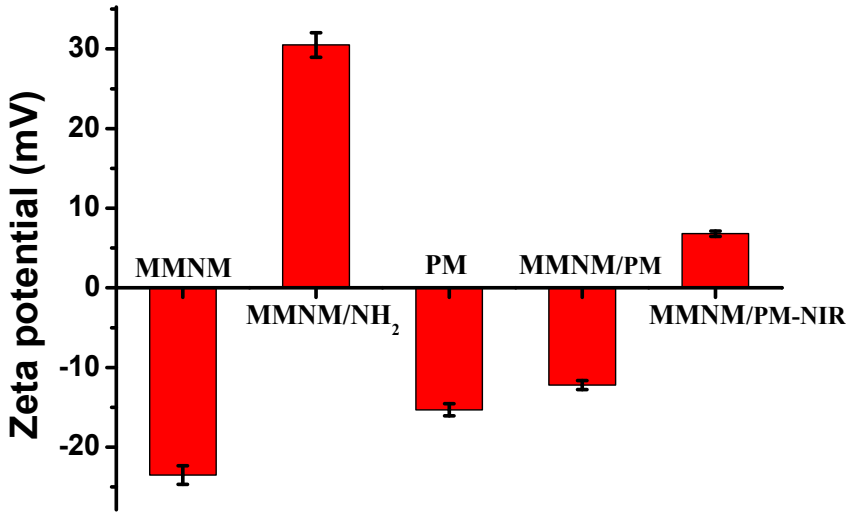

Fig. S7. Zeta potential of different samples.

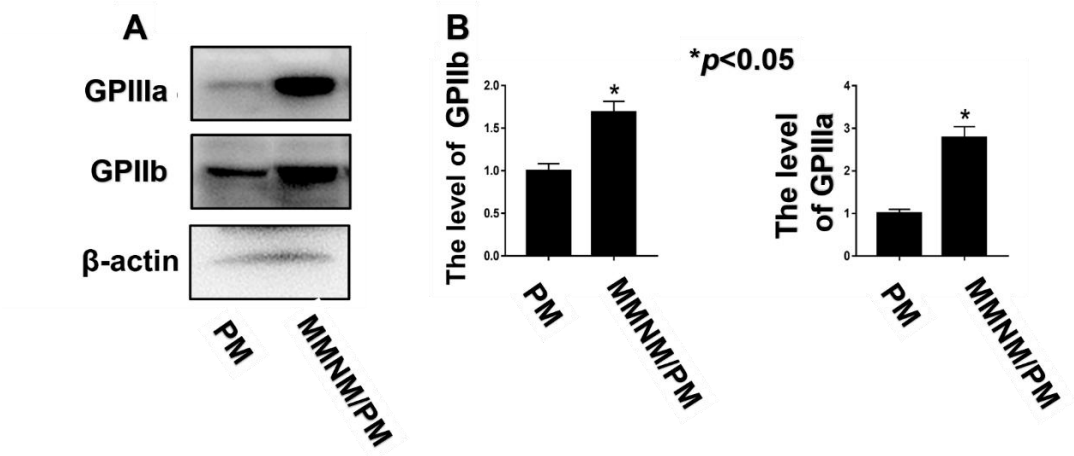

Fig. S8. Western blot assay. (A) Assessment of the proteins by Western blot, and (B) the relative expression level of GP IIb-IIIa receptor molecules on PM and MMNM/PM.

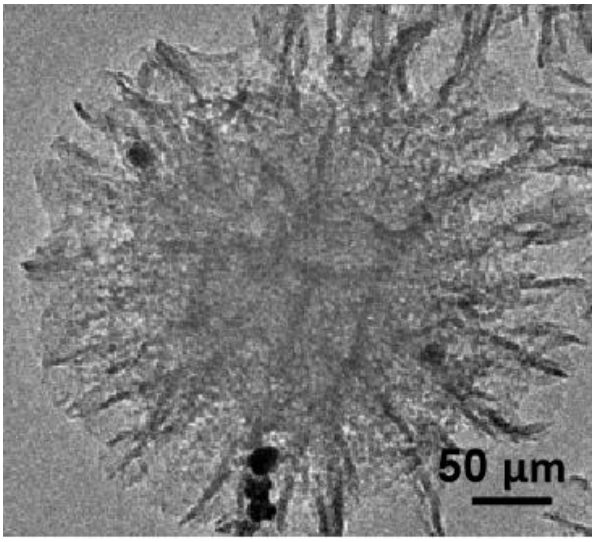

Fig. S9. TEM image of MMNM/PM after being irradiation by NIR for 10 min.

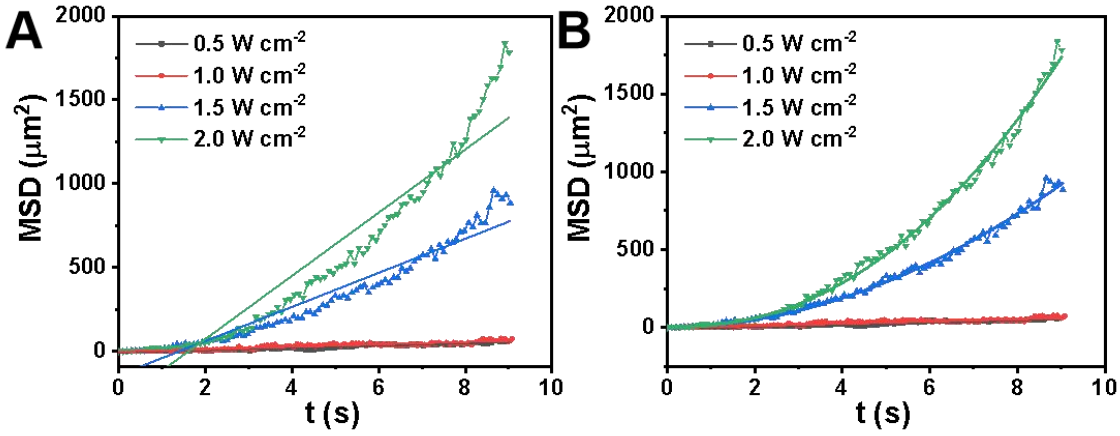

Fig. S10. Motion behavior analysis. (A) Linear ($y = a + bx$) and (B) power function ($y = ax^b$) fitting parameters for MSD plot under different NIR power densities.

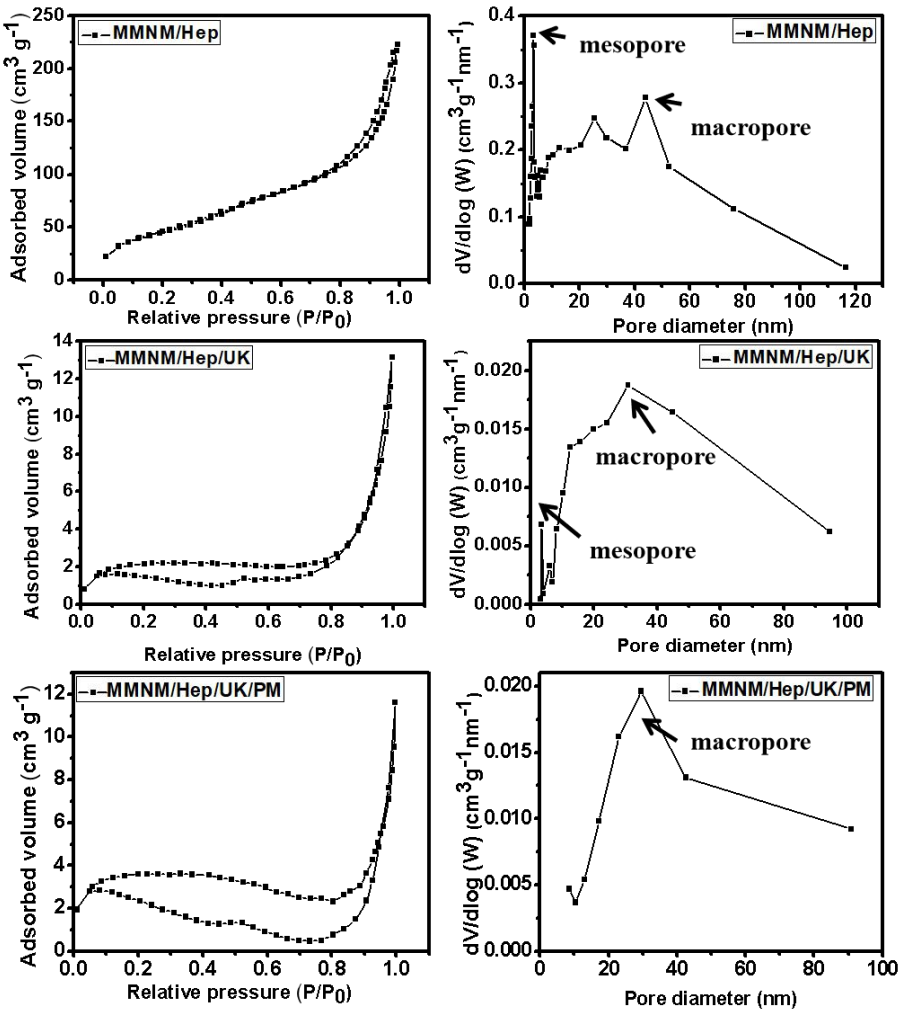

Fig. S11. Pore structure characterization of MMNM loaded with drugs. (left) N_2 adsorption-desorption isotherms and (right) BJH pore size distribution curves of different samples.

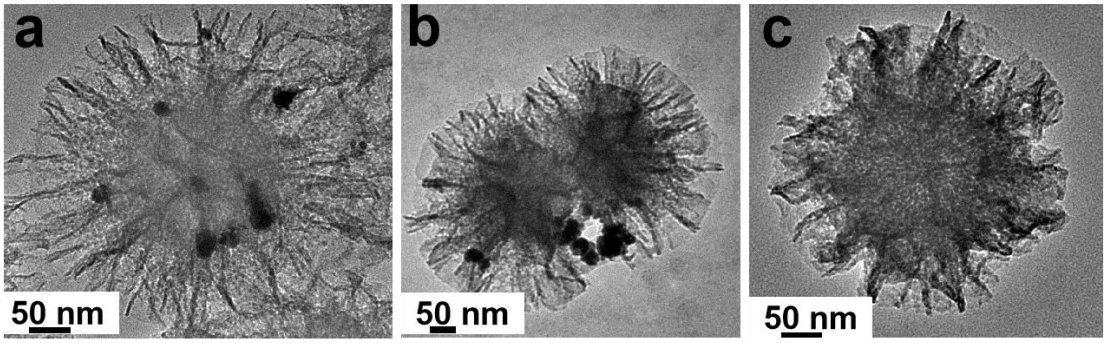

Fig. S12. TEM images of (a) MMNM/Hep, (b) MMNM/Hep/UK and (c) MMNM/Hep/UK/PM.

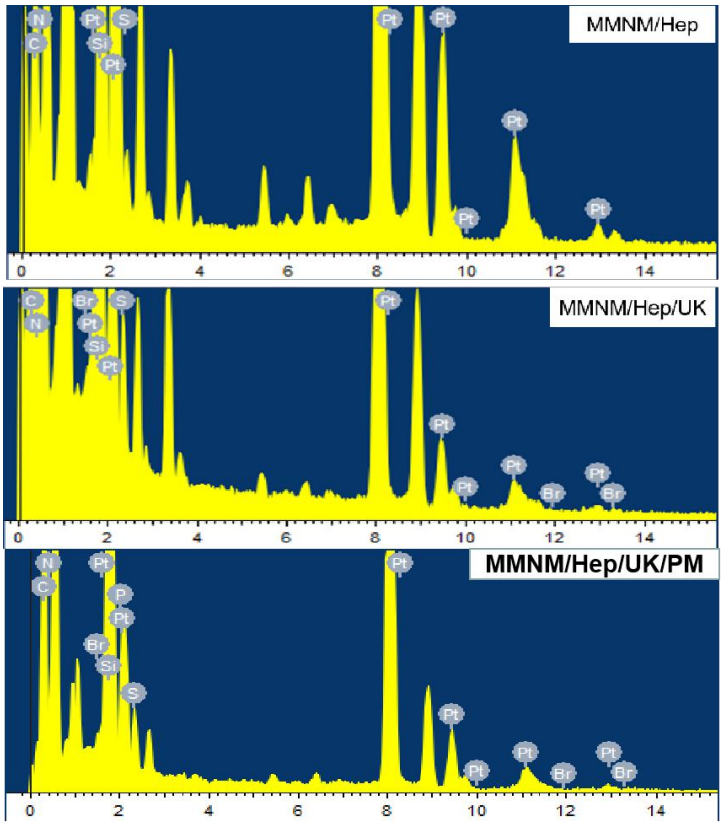

Fig. S13. EDS spectra of different samples.

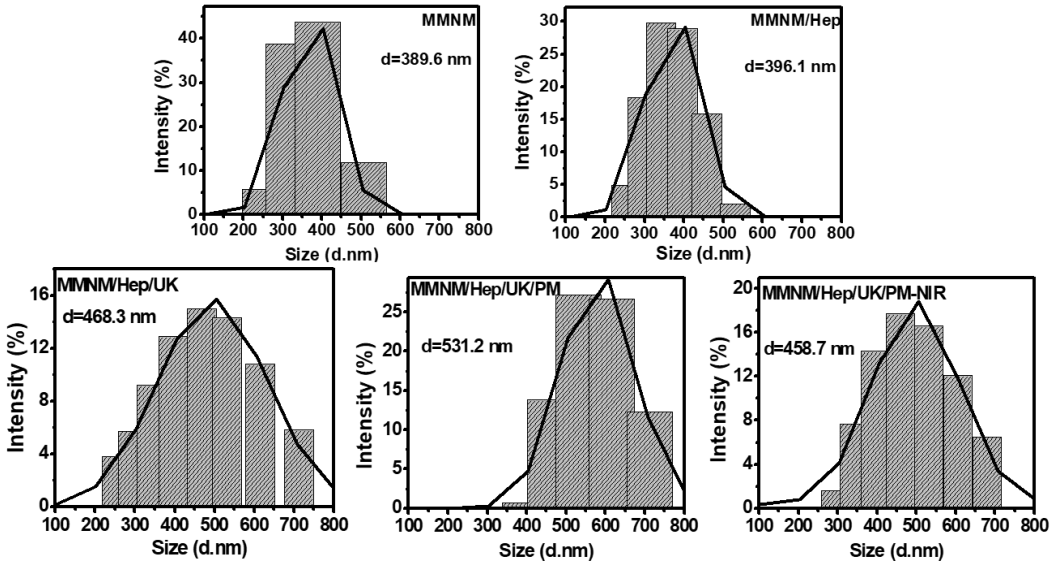

Fig. S14. Dynamic light scattering (DLS) of different samples.

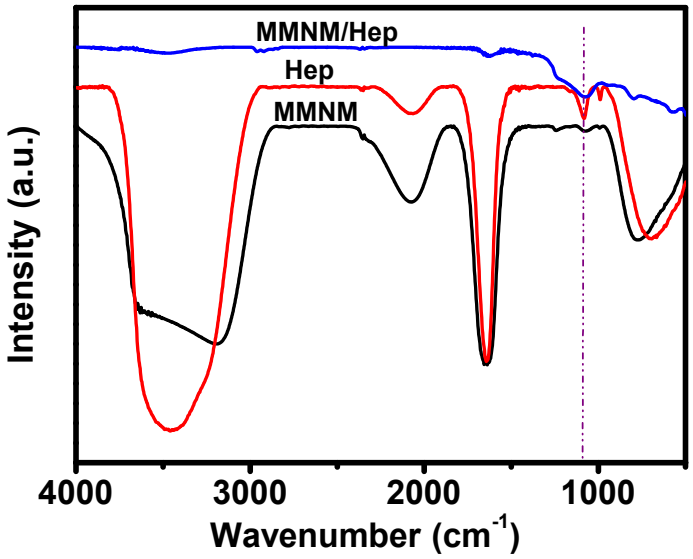

Fig. S15. FTIR spectra of different samples.

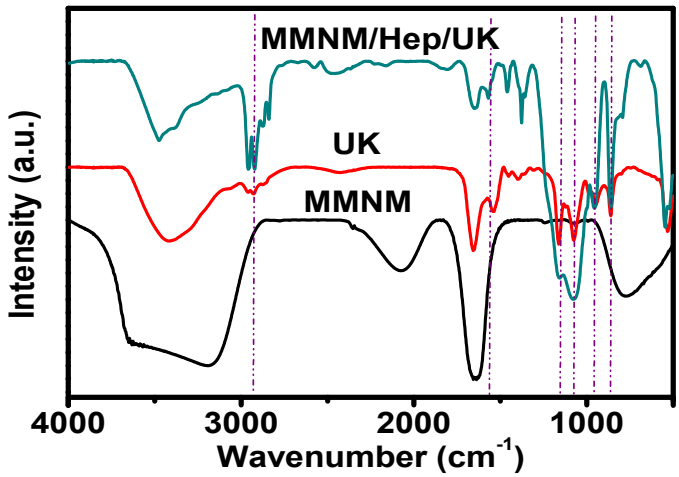

Fig. S16. FTIR spectra of different samples.

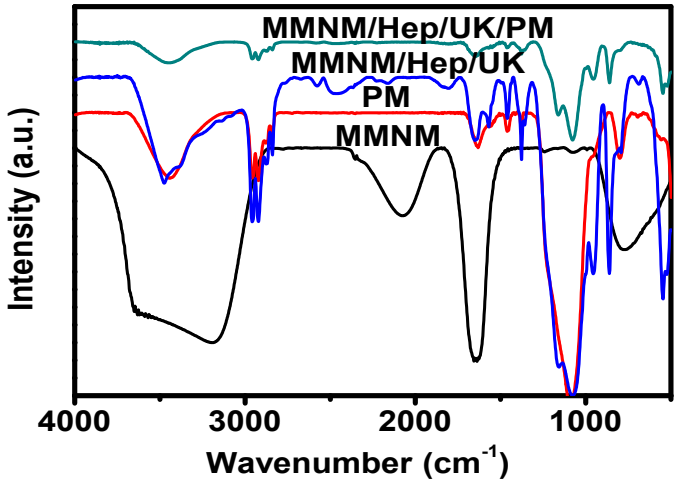

Fig. S17. FTIR spectra of different samples.

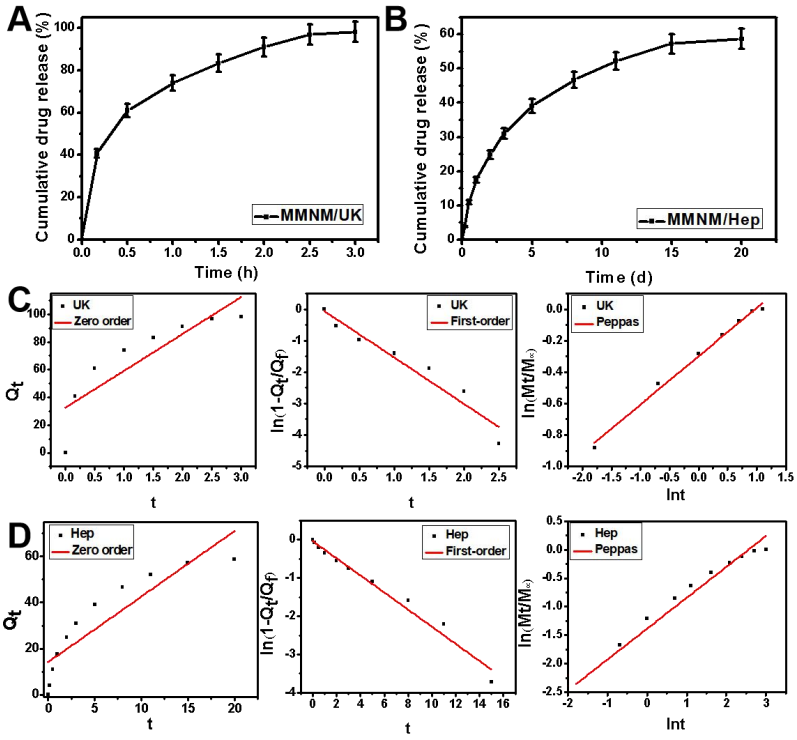

Fig. S18. Drug release analysis. The cumulative release profiles of (A) UK from MMNM/UK and (B) Hep from MMNM/Hep *in vitro*; the release kinetics of (C) UK from MMNM/UK and (D) Hep from MMNM/Hep (Zero-order release model, First-order release model and Peppas release model). Experimental data are mean +/- s.d. of samples in a representative experiment (n=3).

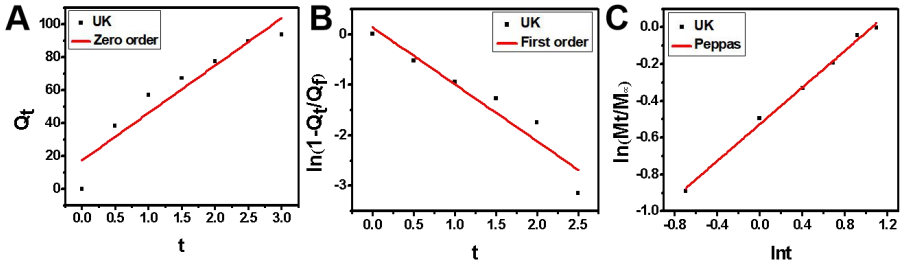

Fig. S19. Drug release analysis. The release kinetics of UK from MMNM/Hep/UK/PM with NIR irradiation (A: Zero-order release model, B: First-order release model, and C: Peppas release model).

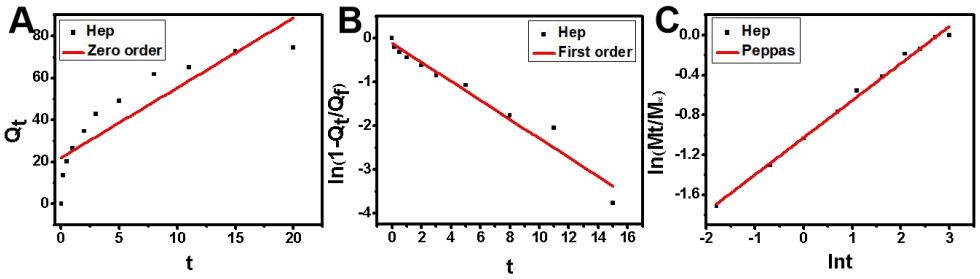

Fig. S20. Drug release analysis. The release kinetics of Hep from MMNM/Hep/UK/PM with NIR irradiation (A: Zero-order release model, B: First-order release model, and C: Peppas release model).

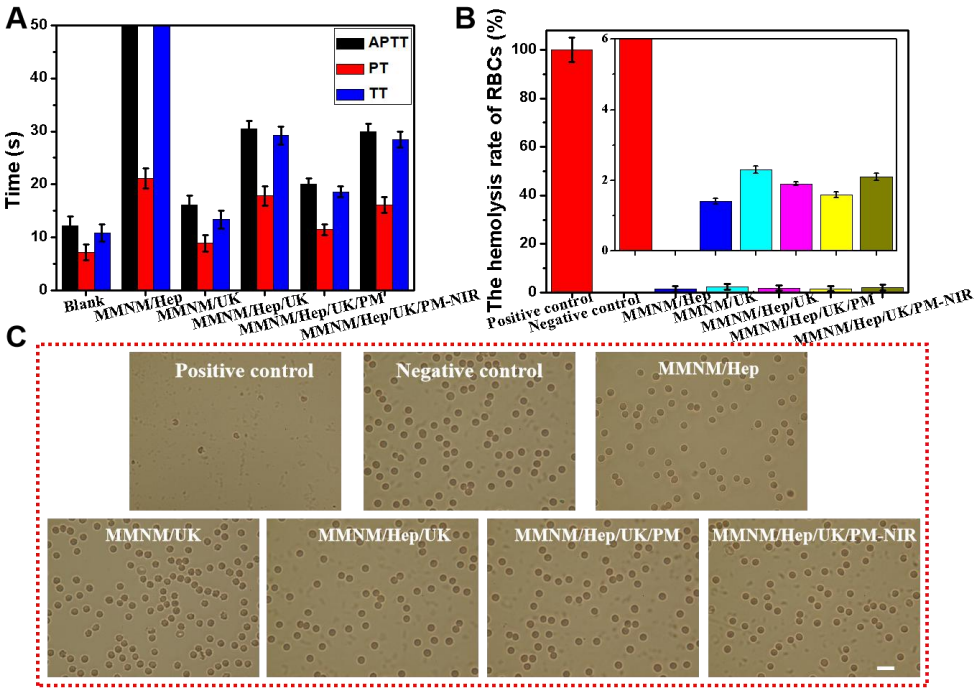

Fig. S21. *In vitro* anticoagulability and blood compatibility of nanomotor. (A) Coagulation time, (B) the hemolysis rates for different samples under different conditions and (C) their corresponding optical images of RBCs (scale bar: 10 μm). Experimental data are mean +/- s.d. of samples in a representative experiment (n=3).

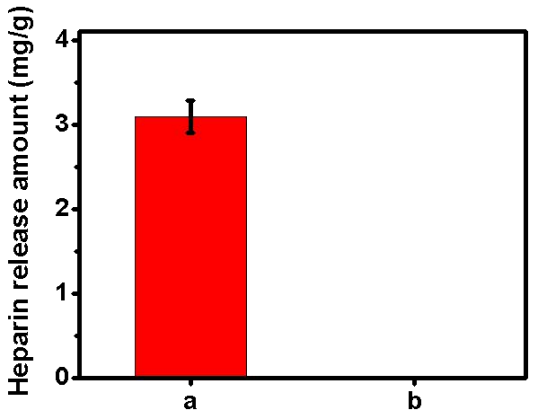

Fig. S22. The amount of Hep released in different samples for the first 1 h: (a) MMNM/Hep, and (b) MMNM/Hep/UK. Experimental data are mean +/- s.d. of samples in a representative experiment (n=3).

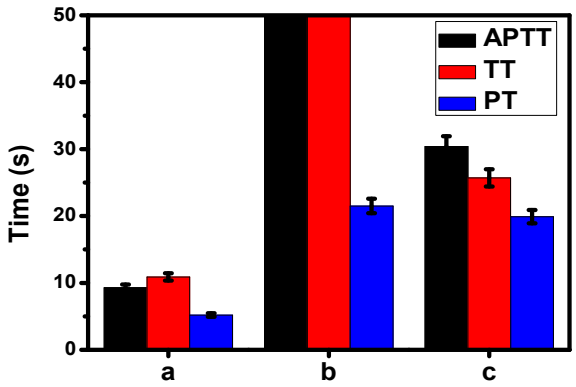

Fig. S23. Anticoagulant properties of the released Hep solution from (a) PBS, (b) MMNM/Hep, and (c) MMNM/Hep/UK for 1 h. Experimental data are mean +/- s.d. of samples in a representative experiment (n=3).

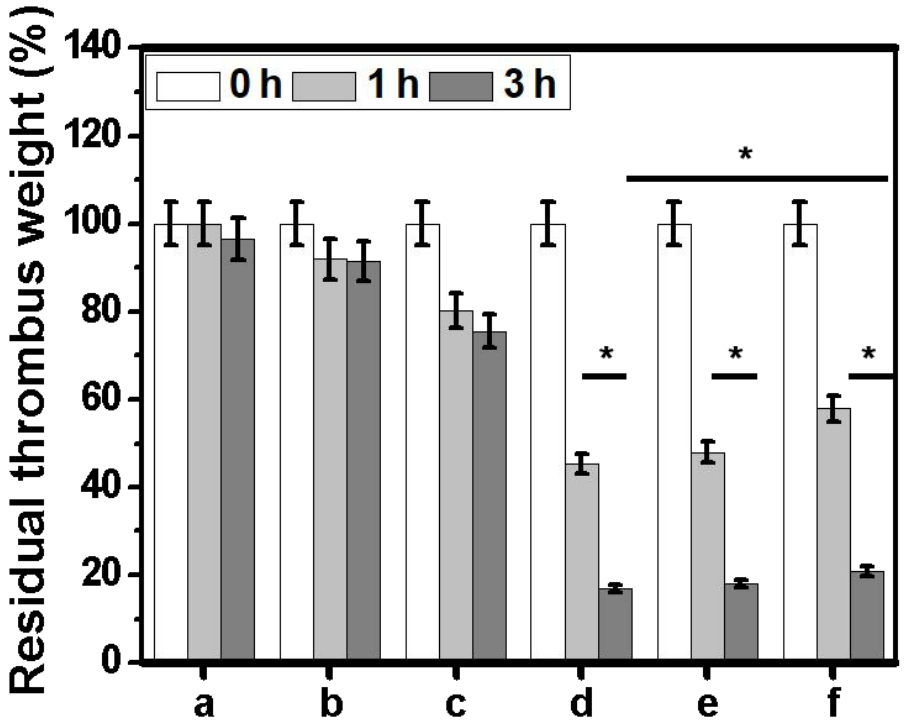

Fig. S24. The residual thrombus weight in static thrombolysis model (a: PBS, b: MMNM, c: MMNM/Hep, d: MMNM/UK, e: MMNM/Hep/UK, and f: MMNM/Hep/UK/PM). An asterisk denotes statistical significance between bars (*P < 0.05) using one-way ANOVA analysis. Experimental data are mean +/- s.d. of samples in a representative experiment (n=3).

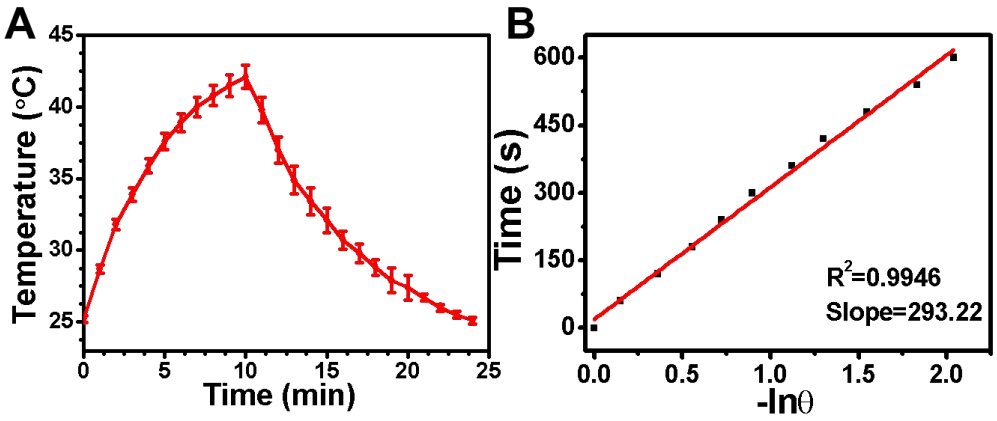

Fig. S25. (A) The relationship between temperature and time of MMNM solution after NIR irradiation for 10 min and laser shutdown to room temperature (808 nm, 2.5 W cm^{-2}); (B) the relationship between negative natural logarithm function of temperature at cooling stage and cooling time. Experimental data are mean +/- s.d. of samples in a representative experiment (n=3).

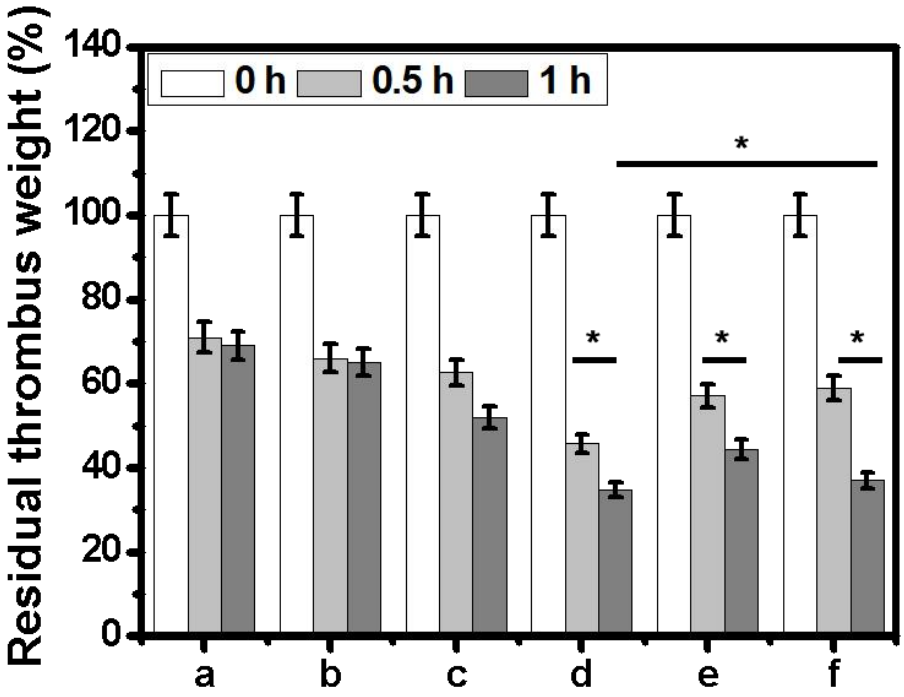

Fig. S26. The residual thrombus weight in dynamic thrombolysis model (a: PBS, b: MMNM, c: MMNM/Hep, d: MMNM/UK, e: MMNM/Hep/UK, and f: MMNM/Hep/UK/PM). An asterisk denotes statistical significance between bars (*P < 0.05) using one-way ANOVA analysis. Experimental data are mean +/- s.d. of samples in a representative experiment (n=3).

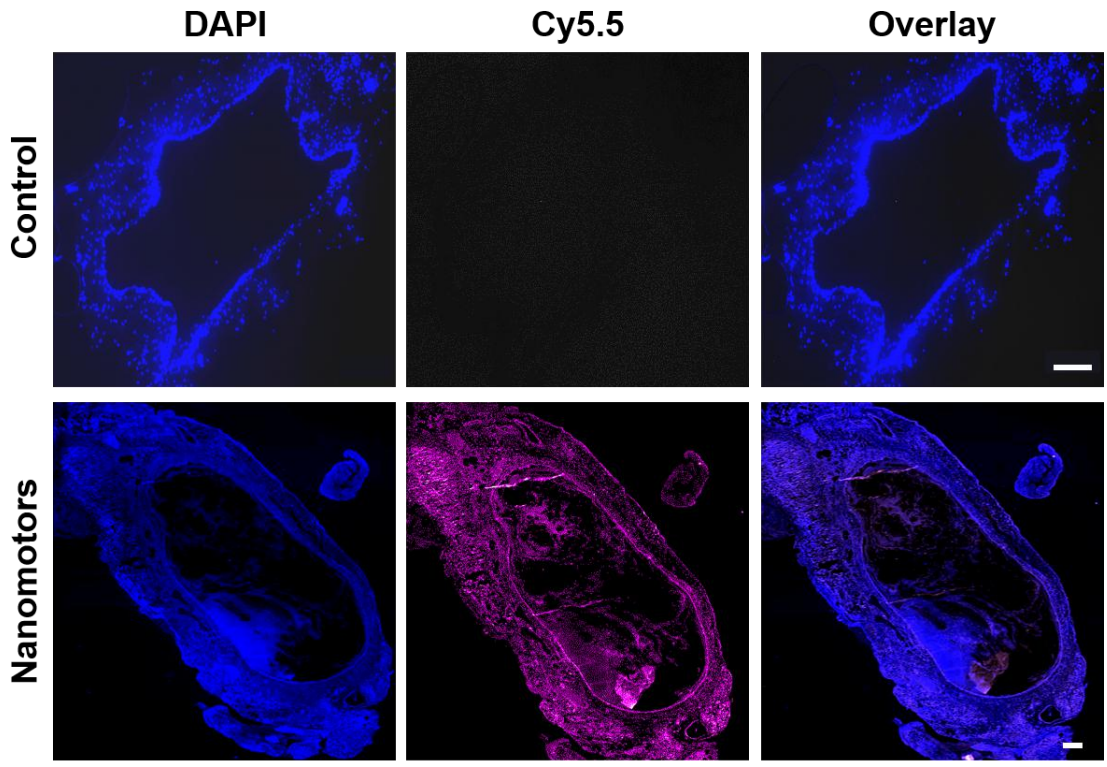

Fig. S27. Freezing microtome section of blood vessels of the control group and after the nanomotors targeting blood vessel-thrombosis for 24 h (Blue: DAPI, Red: MMNM-Cy5.5) (Scale bar: 200 μm).

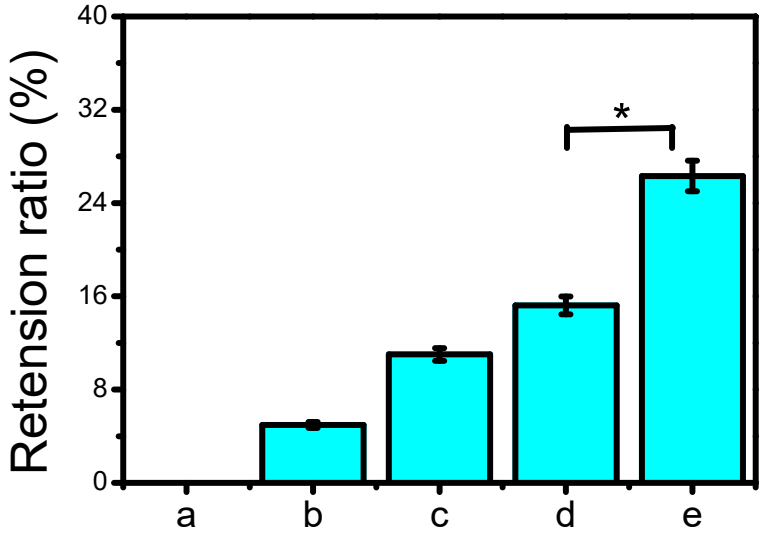

Fig. S28. Retention ratio of (a) Cy5.5, (b) MMNM-Cy5.5, (c) MMNM-Cy5.5+NIR, (d) MMNM/PM-Cy5.5, and (e) MMNM/PM-Cy5.5+NIR irradiation after being injected *in vivo* for 24 h. An asterisk denotes statistical significance between bars (*$P < 0.05$) using one-way ANOVA analysis. Experimental data are mean +/- s.d. of samples in a representative experiment (n=3).

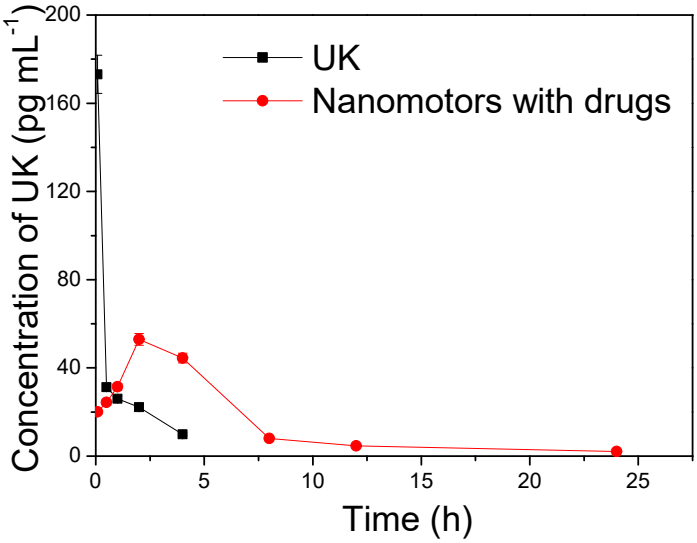

Fig. S29. Drug dynamics of UK *in vivo* for pure UK and nanomotors with drugs. Experimental data are mean +/- s.d. of samples in a representative experiment (n=3).

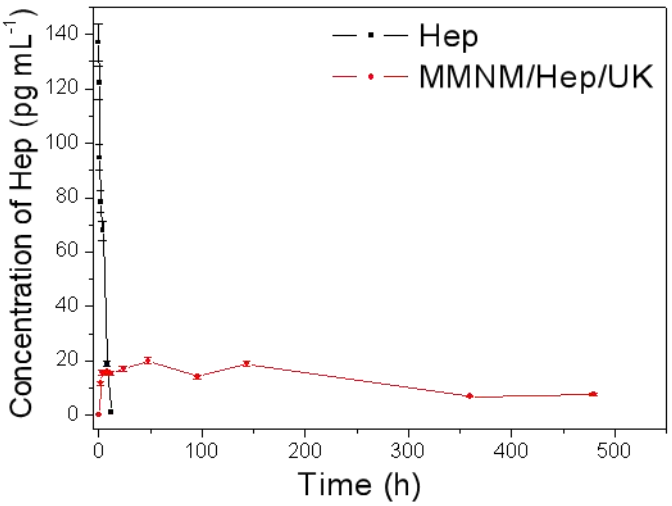

Fig. S30. Drug dynamics of Hep *in vivo* for pure Hep and nanomotors with drugs. Experimental data are mean +/- s.d. of samples in a representative experiment (n=3).

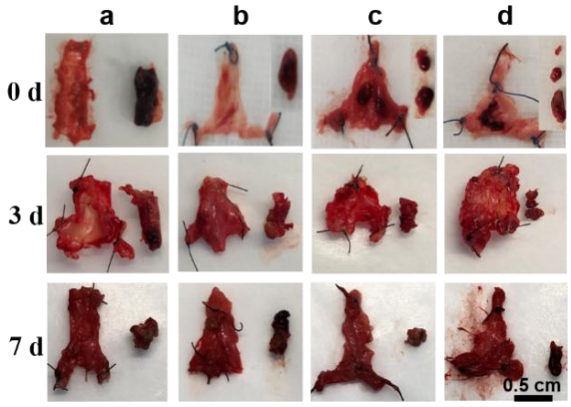

Fig. S31. Photographs of blood vessels and thrombus at 0 d, 3 d, and 7 d of different samples (a: MMNM/UK, b: MMNM/Hep, c: MMNM/Hep/UK, d: MMNM/Hep/UK/PM). (Photo Credit: Rongliang Wang and Rui Wu, Department of Sports Medicine and Adult Reconstructive Surgery, Nanjing Drum Tower Hospital, The Affiliated Hospital of Nanjing University Medical School, Nanjing, 210008, China.)

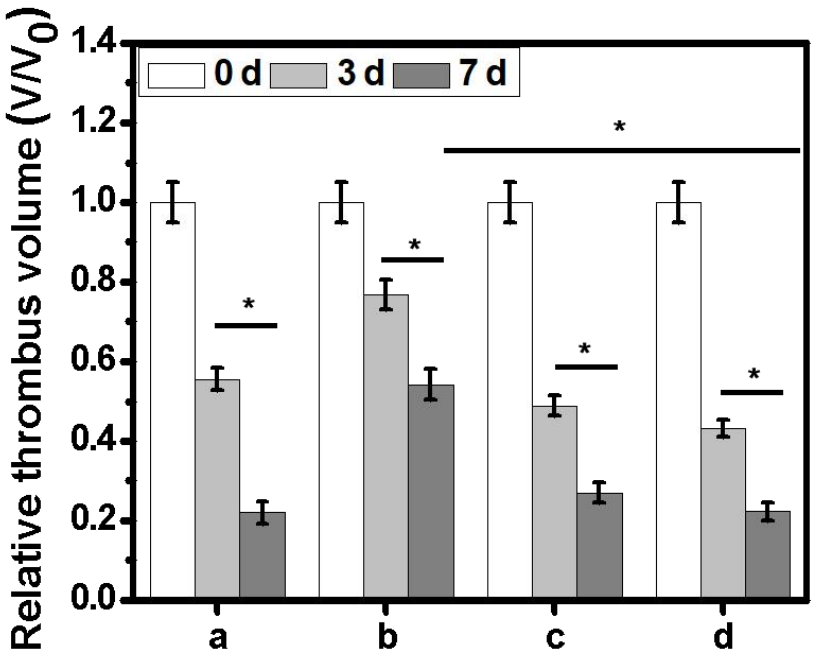

Fig. S32. Relative volume of thrombus after being treated with different samples for 0, 3 and 7 d (a: MMNM/UK, b: MMNM/Hep, c: MMNM/Hep/UK, d: MMNM/Hep/UK/PM). An asterisk denotes statistical significance between bars (*P < 0.05) using one-way ANOVA analysis. Experimental data are mean +/- s.d. of samples in a representative experiment (n=3).

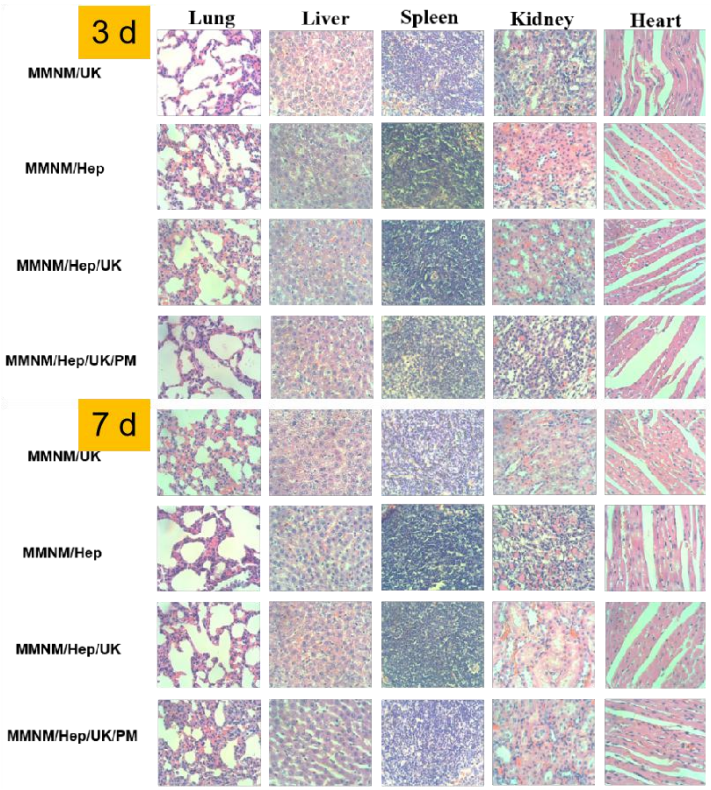

Fig. S33. H&E sections and staining of major organs of rats after 3 and 7 d of thrombolysis (400×).

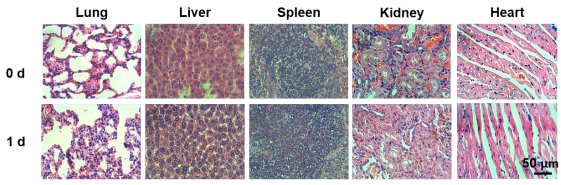

Fig. S34. H&E sections and staining of major organs of rats after being treated with nanomotors for 1 d.

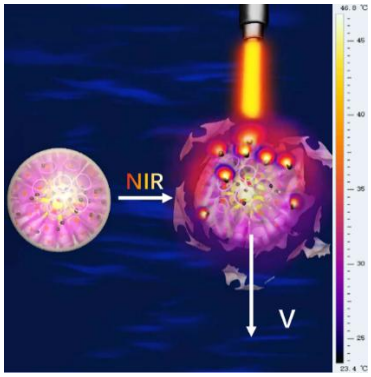

Fig. S35. Possible mechanism for the motion of nanomotors under NIR irradiation.

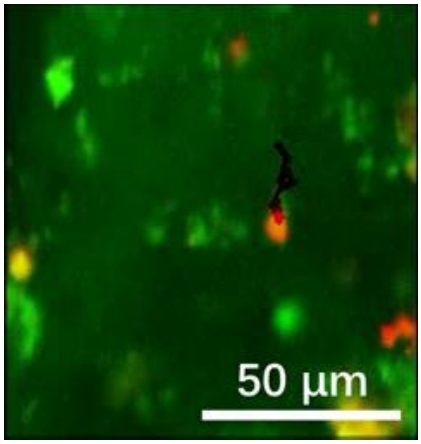

Fig. S36. Time-lapsed CLSM images of fluorescent floating fibrin clots in the presence of nanomotors upon NIR irradiation (Movie S2, 808 nm, 5 s) (Green color: fluorescent floating fibrin clots stained by FITC, Red color: nanomotors stained with Cy5.5).

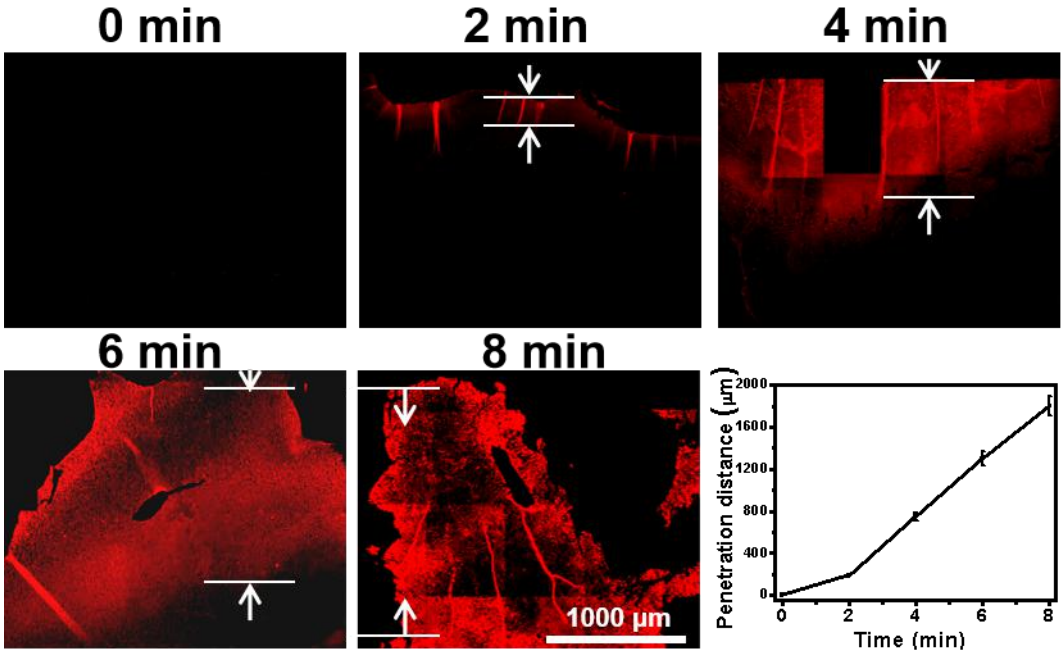

Fig. S37. The longitudinal section of the thrombus after being treated with Cy5.5-stained nanomotors under NIR irradiation for different time and corresponding penetration distance. Experimental data are mean +/- s.d. of samples in a representative experiment (n=3).

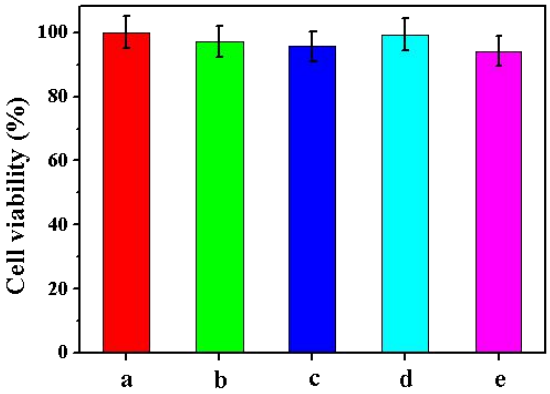

Fig. S38. Cell viabilities of HUVECs treated with different samples. (a: blank; b: MMNM; c: MMNM/Hep/UK; d: MMNM/Hep/UK/PM, e: MMNM/Hep/UK/PM+NIR irradiation). Experimental data are mean +/- s.d. of samples in a representative experiment (n=3).

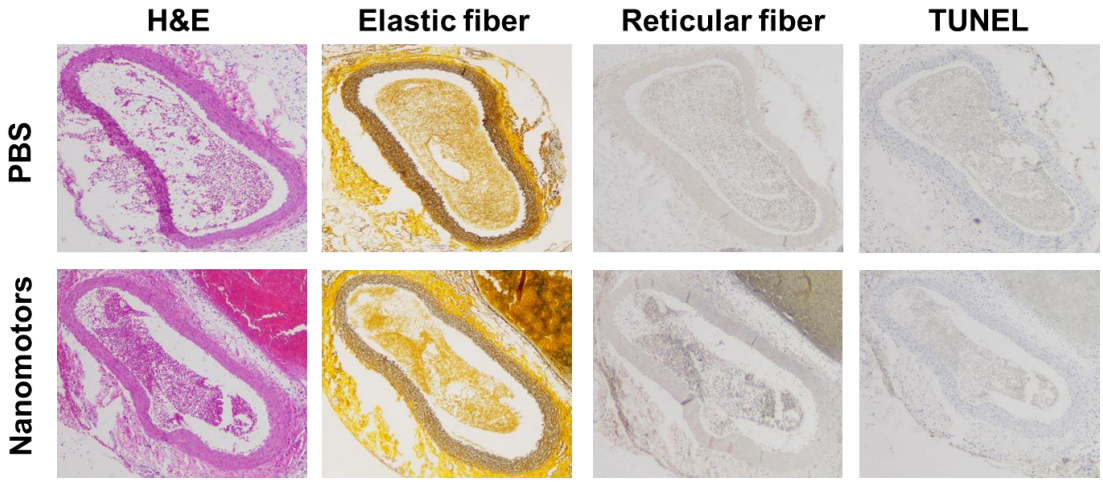

Fig. S39. Cross-sectional histology of rat blood vessels (stained with H&E, elastic fiber staining, reticular fiber staining, TUNEL, 40×).

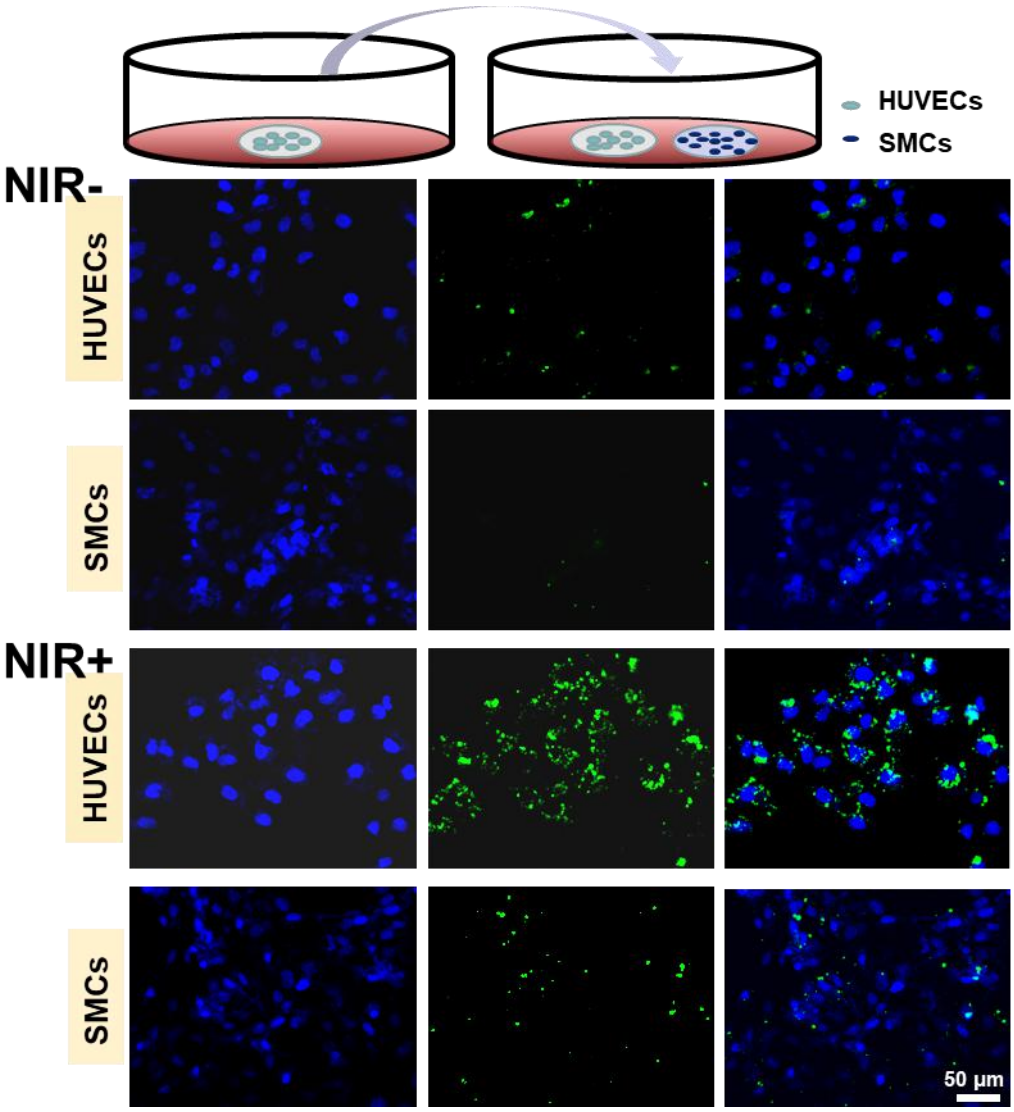

Fig. S40. Schematic illustration and CLSM images of MMNM/FITC/PM nanomotors *in vitro* experimental models from HUVECs to SMCs with or without NIR irradiation (Blue color: DAPI, nucleus; Green color: nanomotors stained with FITC).

REFERENCES AND NOTES

1. A. S. Go, D. Mozaffarian, V. L. Roger, E. J. Benjamin, J. D. Berry, M. J. Blaha, S. Dai, E. S. Ford, C. S. Fox, S. Franco, H. J. Fullerton, C. Gillespie, S. M. Hailpern, J. A. Heit, V. J. Howard, M. D. Huffman, S. E. Judd, B. M. Kissela, S. J. Kittner, D. T. Lackland, J. H. Lichtman, L. D. Lisabeth, R. H. Mackey, D. J. Magid, G. M. Marcus, A. Marelli, D. B. Matchar, D. K. McGuire, E. R. Mohler, C. S. Moy, M. E. Mussolino, R. W. Neumar, G. Nichol, D. K. Pandey, N. P. Paynter, M. J. Reeves, P. D. Sorlie, J. Stein, A. Towfighi, T. N. Turan, S. S. Virani, N. D. Wong, D. Woo, M. B. Turner; American Heart Association Statistics Committee and Stroke Statistics Subcommittee, Executive summary: Heart disease and stroke statistics-2014 update a report from the american heart association. *Circulation* **129**, 399–410 (2014).

2. J. A. Heit, F. A. Spencer, R. H. White, The epidemiology of venous thromboembolism. *J. Thromb. Thrombolysis* **41**, 3–14 (2016).

3. J. A. Heit, Epidemiology of venous thromboembolism. *Nat. Rev. Cardiol.* **12**, 464–474 (2015).

4. R. Lecumberri, A. Alfonso, D. Jimenez, C. Fernandez Capitan, P. Prandoni, P. S. Wells, G. Vidal, G. Barillari, M. Monreal; RIETE investigators, Dynamics of case-fatalilty rates of recurrent thromboembolism and major bleeding in patients treated for venous thromboembolism. *Thromb. Haemost.* **110**, 834–843 (2013).

5. G. W. Landman, R. O. Gans, Oral rivaroxaban for symptomatic venous thromboembolism. *N. Engl. J. Med.* **364**, 1178 (2011).

6. R. S. Marshall, Progress in intravenous thrombolytic therapy for acute stroke. *JAMA Neurol.* **72**, 928–934 (2015).

7. M. Juenet, R. Aid-Launais, B. Li, A. Berger, J. Aerts, V. Ollivier, A. Nicoletti, D. Letourneur, C. Chauvierre, Thrombolytic therapy based on fucoidan-functionalized polymer nanoparticles targeting P-selectin. *Biomaterials* **156**, 204–216 (2018).

8. H. Kobayashi, R. Watanabe, P. L. Choyke, Improving conventional enhanced permeability and retention (EPR) effects; what is the appropriate target? *Theranostics* **4**, 81–89 (2013).

9. Z. J. Chen, T. Xia, Z. L. Zhang, S. Z. Xie, T. Wang, X. H. Li, Enzyme-powered Janus nanomotors launched from intratumoral depots to address drug delivery barriers. *Chem. Eng. J.* **375**, 122109 (2019).

10. X. Ma, S. Jang, M. N. Popescu, W. E. Uspal, A. Miguel-López, K. Hahn, D-P.. Kim, S. Sánchez, Reversed Janus micro/nanomotors with internal chemical engine. *ACS Nano* **10**, 8751–8759 (2016).

11. M. Xuan, Z. Wu, J. Shao, L. Dai, T. Si, Q. He, Near infrared light-powered Janus mesoporous silica nanoparticle motors. *J. Am. Chem. Soc.* **138**, 6492–6497 (2016).

12. J. Shao, M. Abdelghani, G. Shen, S. Cao, D. S. Williams, J. C. M. van Hest, Erythrocyte membrane modified Janus polymeric motors for thrombus therapy. *ACS Nano* **12**, 4877–4885 (2018).

13. EINSTEIN Investigators, R. Bauersachs, S. D. Berkowitz, B. Brenner, H. R. Buller, H. Decousus, A. S. Gallus, A. W. Lensing, F. Misselwitz, M. H. Prins, G. E. Raskob, A. Segers, P. Verhamme, P. Wells, G. Agnelli, H. Bounameaux, A. Cohen, B. L. Davidson, F. Piovella, S. Schellong, Oral rivaroxaban for symptomatic venous thromboembolism. *N. Engl. J. Med.* **363**, 2499–2510 (2010).

14. B. A. Hutten, M. H. Prins, Duration of treatment with vitamin K antagonists in symptomatic venous thromboembolism. *Cochrane Database Syst. Rev.* **1**, CD001367 (2006).

15. Y. X. Yang, J. B. Zhang, W. M. Yang, J. D. Wu, R. S. Chen, Adsorption properties for urokinase on local diatomite surface. *Appl. Surf. Sci.* **206**, 20–28 (2003).

16. B. Mulloy, S. Khan, S. J. Perkins, Molecular architecture of heparin and heparan sulfate: Recent developments in solution structural studies. *Pure Appl. Chem.* **84**, 65–76 (2012).

17. Z. W. Chen, Q. Y. Hu, Z. Gu, Leveraging engineering of cells for drug delivery. *Acc. Chem. Res.* **51**, 668–677 (2018).

18. Y. F. Lu, Q. Y. Hu, C. Jiang, Z. Gu, Platelet for drug delivery. *Curr. Opin. Biotechnol.* **58**, 81–91 (2019).

19. Q. Y. Hu, C. G. Qian, W. J. Sun, J. Q. Wang, Z. W. Chen, H. N. Bomba, H. L. Xin, Q. D. Shen, Z. Gu, Engineered nanoplatelets for enhanced treatment of multiple myeloma and thrombus. *Adv. Mater.* **28**, 9573–9580 (2016).

20. Z. G. Wu, X. K. Lin, Y. J. Wu, T. Y. Si, J. M. Sun, Q. He, Near-infrared light-triggered "on/off" motion of polymer multilayer rockets. *ACS Nano* **8**, 6097–6105 (2014).

21. N. Zhang, M. H. Li, X. T. Sun, H. Z. Jia, W. G. Liu, NIR-responsive cancer cytomembrane-cloaked carrier-free nanosystems for highly efficient and self-targeted tumor drug delivery. *Biomaterials* **159**, 25–36 (2018).

22. J. P. Xu, X. Q. Wang, H. Y. Yin, X. Cao, Q. Y. Hu, W. Lv, Q. W. Xu, Z. Gu, H. L. Xin, Sequentially site-specific delivery of thrombolytics and neuroprotectant for enhanced treatment of ischemic stroke. *ACS Nano* **13**, 8577–8588 (2019).

23. Q. Y. Hu, W. J. Sun, C. G. Qian, C. Wang, H. N. Bomba, Z. Gu, Anticancer platelet-mimicking manovehicles. *Adv. Mater.* **27**, 7043–7050 (2015).

24. M. J. Xuan, R. Mestre, C. Y. Gao, C. Zhou, Q. He, S. Sánchez, Noncontinuous super-diffusive dynamics of a light-activated nanobottle motor. *Angew. Chem. Int. Ed.* **57**, 6838–6842 (2018).

25. Q. Wang, S. L. Hu, Y. B. Wu, Q. Niu, Y. Y. Huang, F. Wu, X. T. Zhu, J. Fan, G. Y. Yin, M. M. Wan, C. Mao, M. Zhou, Multiple drug delivery from mesoporous coating realizing combination therapy for bare metal stents. *Langmuir* **35**, 3126–3133 (2019).

26. R. F. Luo, J. Zhang, W. H. Zhuang, L. Deng, L. H. Li, H. C. Yu, J. Wang, N. Huang, Y. B. Wang, Multifunctional coatings that mimic the endothelium: surface bound active heparin nanoparticles with in situ generation of nitric oxide from nitrosothiols. *J. Mater. Chem. B* **6**, 5582–5595 (2018).

27. V. Dubovoy, A. Ganti, T. Zhang, H. Al-Tameemi, J. D. Cerezo, J. M. Boyd, T. Asefa, One-pot hydrothermal synthesis of benzalkonium-templated mesostructured silica antibacterial agents. *J. Am. Chem. Soc.* **140**, 13534–13537 (2018).

28. H. P. Sun, J. H. Su, Q. S. Meng, Q. Yin, L. L. Chen, W. W. Gu, Z. W. Zhang, H. J. Yu, P. C. Zhang, S. L. Wang, Y. P. Li, Cancer cell membrane coated gold nanocages with hyperthermia-triggered drug release and homotypic target inhibit growth and metastasis of breast cancer. *Adv. Funct. Mater.* **27**, 1604300 (2017).

29. J. Shi, M. Y. Wang, Z. Sun, Y. Y. Liu, J. N. Guo, H. L. Mao, F. Yan, Aggregation-induced emission-based ionic liquids for bacterial killing, imaging, cell labeling, and bacterial detection in blood cells. *Acta Biomater.* **97**, 247–259 (2019).

30. H. Chen, X. B. Wang, Q. Zhou, P. Xu, Y. Liu, M. Wan, M. Zhou, C. Mao, Preparation of vascular endothelial cadherin loaded-amphoteric copolymer decorated coronary stents for anticoagulation and endothelialization. *Langmuir* **33**, 13430–13437 (2017).

31. X. L. Wang, C. C. Wei, M. K. Liu, T. Yang, W. M. Zhou, Y. Liu, K. Hong, S. H. Wang, H. B. Xin, X. W. Ding, Near-infrared triggered release of uPA from nanospheres for localized hyperthermia-enhanced thrombolysis. *Adv. Funct. Mater.* **27**, 1701824 (2017).

32. N. Korin, M. Kanapathipillai, B. D. Matthews, M. Crescente, A. Brill, T. Mammoto, K. Ghosh, S. Jurek, S. A. Bencherif, D. Bhatta, A. U. Coskun, C. L. Feldman, D. D. Wagner, D. E. Ingber, Shear-activated nanotherapeutics for drug targeting to obstructed blood vessels. *Science* **337**, 738–742 (2012).

33. J. A. Diaz, A. T. Obi, D. D. Myers, J. S. K. Wrobleski, P. K. Henke, N. Mackman, T. W. Wakefield, Critical review of mouse models of venous thrombosis. *Arterioscler. Thromb. Vasc. Biol.* **32**, 556–562 (2012).

34. Z. X. Lu, F. Y. Huang, R. Cao, G. H. Tan, G. H. Yi, N. Y. He, L. F. Xu, L. M. Zhang, Intrinsic, cancer cell-selective toxicity of organic photothermal nanoagent: a simple formulation for combined photothermal chemotherapy of cancer. *ACS Appl. Mater. Interfaces* **10**, 26028–26038 (2018).

35. S. Koudelka, R. Mikulik, J. Mašek, M. Raška, P. T. Knotigová, A. D.Miller, J. Turánek, Liposomal nanocarriers for plasminogen activators. *J. Control. Release* **227**, 45–57 (2016).

36. J. Martínez-González, L. Vila, C. Rodríguez, Bemiparin: second-generation, low-molecular-weight heparin for treatment and prophylaxis of venous thromboembolism. *Expert. Rev. Cardiovasc. Ther.* **6**, 793–802 (2008).

37. F. Peng, Y. J. Men, Y. F. Tu, Y. M. Chen, D. A. Wilson, Nanomotor-based strategy for enhanced penetration across vasculature model. *Adv. Funct. Mater.* **28**, 1706117 (2018).

38. M. Luo, Y. Z. Feng, T. W. Wang, J. G. Guan, Micro-/Nanorobots at work in active drug delivery. *Adv. Funct. Mater.* **28**, 1706100 (2018).

39. T. W. Chung, S. S. Wang, W. J. Tsai, Accelerating thrombolysis with chitosan-coated plasminogen activators encapsulated in poly-(lactide-co-glycolide) (PLGA) nanoparticles. *Biomaterials* **29**, 228–237 (2008).

40. J. Xu, J. Zhou, Y. X. Zhong, Y. Zhang, J. Liu, Y. L. Chen, L. M. Deng, D. L. Sheng, Z. G. Wang, H. T. Ran, D. J. Guo, Phase transition nanoparticles as multimodality contrast agents for the detection of thrombi and for targeting thrombolysis: *in vitro* and *in vivo* experiments. *ACS Appl. Mater. Interfaces* **9**, 42525–42535 (2017).

41. A. S. Wolberg, Thrombin generation and fibrin clot structure. *Blood Rev.* **21**, 131–142 (2007).

42. M. H. Kural, J. Wang, L. Q. Gui, Y. F. Yuan, G. X. Li, K. L. Leiby, E. Quijano, G. Tellides, W. M. Saltzman, L. E. Niklason, Fas ligand and nitric oxide combination to control smooth muscle growth while sparing endothelium. *Biomaterials* **212**, 28–38 (2019).

43. P. L. Abbaraju, A. K. Mek, H. Song, Y. N. Yang, M. Jambhrunkar, J. Zhang, C. Xu, M. H. Yu, C. Z. Yu, Asymmetric silica nanoparticles with tunable head-tail structures enhance hemocompatibility and maturation of immune cells. *J. Am. Chem. Soc.* **139**, 6321–6328 (2017).

44. T. Yang, X. Ding, L. Dong, C. Hong, J. Ye, Y. Xiao, X. Wang, H. Xin, Platelet-mimic uPA delivery nanovectors based on Au rods for thrombus targeting and treatment. *ACS Biomater Sci. Eng.* **4**, 4219–4224 (2018).

45. Y. L. Liu, K. L. Ai, J. H. Liu, M. Deng, Y. Y. He, L. H. Lu, Dopamine-melanin colloidal nanospheres: an efficient near-infrared photothermal therapeutic agent for in vivo cancer therapy. *Adv. Mater.* **25**, 1353–1359 (2013).

46. W. Z. Ren, Y. Yan, L. Y. Zeng, Z. Z. Shi, A. Gong, P. Schaaf, D. Wang, J. S. Zhao, B. B. Zou, H. S. Yu, G. Chen, E. M. B. Brown, A. G. Wu, A near infrared light triggered hydrogenated black TiO_2 for cancer photothermal therapy. *Adv. Healthc. Mater.* **4**, 1526–1536 (2015).